Mon. Not. R. Astron. Soc. **000**, 1–?? (1999) Printed 9 February 2000 (MN LaTeX style file v1.4)

On measuring low-degree p-mode frequency splitting with full-disc integrated data

T. Appourchaux[1], H-Y. Chang[2], D.O. Gough[3,4,5], T. Sekii[3],
[1] *ESA/ESTEC, P.O. Box 299, 2200 AG, Noordwijk, The Netherlands*
[2] *Korea Institute for Advanced Study, 207-43 Cheongryangri-dong Dongdaemun-gu, Seoul 130-012, Republic of Korea*
[3] *Institute of Astronomy, University of Cambridge, Madingley Road, Cambridge, CB3 0HA, UK*
[4] *Department of Applied Mathematics and Theoretical Physics, University of Cambridge, Silver Street, Cambridge, CB3 9EW, UK*
[5] *Department of Physics, HEPL Annex B208, 455 Via Palou, Stanford, California 94305-4085, USA*

In original form 8 February 2000

ABSTRACT
The standard method of measuring rotational splitting from solar full-disc oscillation data, based on maximum-likelihood fitting of multi-Lorentzian profiles to oscillation power spectra, systematically overestimates the splitting. One of the reasons is that the maximum likelihood estimators (MLE) become unbiased only *asymptotically* as the number of data tends to infinity; for a finite data set they are often biased, inducing a systematic error. In this paper we assess by Monte-Carlo simulations the amount of systematic error in the splitting measurement, using artificially generated power spectra. The simulations are carried out for multiplets of degree $l = 1, 2$ and 3 with various signal-to-noise ratios, linewidths and observing times. We address the possible use of non-MLE estimators that could provide a smaller or negligible systematic error. The implication for asteroseismology is also discussed.

Key words: solar rotation – p modes – maximum-likelihood estimator

1 INTRODUCTION

Low-degree p-mode frequency splitting measurements are of paramount importance to the investigation of the dynamics of the deep interior of the Sun. Until the mid 1990s, such measurements provided by full-disc integrating instruments were the best, owing mainly to the stability of resonance cells. However, inferences from the various analyses of the low-degree data obtained from those instruments (Toutain & Fröhlich 1992; Loudagh et al. 1993; Jiménez et al. 1994; Toutain & Kosovichev 1994; Chaplin et al. 1996) are disparate, the differences being significantly greater than the estimates of the standard errors, suggesting that at least some splitting measurements could suffer from systematic errors.

The differences lead to substantially different inferences about the angular velocity in the Sun's core. The reason is that the sensitivity of the low-degree p modes to rotation below $0.2R_\odot$ is very weak. For example, an increase of 100 nHz in the solar rotational frequency below $0.2R_\odot$ would increase the splitting of the $l = 1, n = 24$ mode by only 4 nHz (l is the degree of the mode, and n the order). With so weak a sensitivity, it is essential that any systematic error in the analysis to infer low-degree splitting must be made as small as possible.

Fortunately, since 1996 we do not have to rely so heavily on full-disc integrating instruments for deriving the splittings of low-degree solar modes. Measurements using imaging instruments such as GONG (Hill et al. 1996), LOWL (Tomczyk, Schou & Thompson 1996), SOI/MDI (Kosovichev et al. 1997) and LOI (Appourchaux et al. 1997) are almost as stable as a resonance cell. These improvements result from a combination of better technology and better measurement strategy. For instance, the building of Michelson interferometers and of magneto-optical filters are considerable improvements, in terms of spectral stability, over spectrometers (Harvey 1986). Moreover, making simultaneous images of the Sun has the advantage over the earlier image-scanning procedures of being less susceptible to spatially coherent terrestrial atmospheric noise (Harvey 1988; Appourchaux et al. 1995; Tomczyk et al. 1995).

The instruments can now achieve better precision and produce smaller systematic errors than they did in the past, as discussed by Appourchaux (1998). Nevertheless, for the most deeply penetrating $l = 1$ modes the full-disc integrating instruments compete favourably with imaging instruments in terms of the magnitude of random errors. Consequently the removal of the systematic errors from analyses of full-disc data remains an important objective, provided it can be achieved without substantially magnifying the random errors.

Even if imaging instruments have provided a good solution to obviating systematic errors in the solar case, they cannot presently do so for other stars. The COROT mission, planned to be flown in 2002, will try to obtain the first rich solar-like p-mode spectra (Baglin et al. 1998). Other similar missions, e.g. MONS (Kjeldsen & Bedding 1998) and MOST (Matthews 1998), are planned. The instruments will observe the full-disc integrated intensities of a variety of stars. In the case of COROT there will not be many observations dedicated to a single star, the duration of the longest time series being about 3 months. Since full-disc intensity observations will provide the only high-quality asteroseismic data for some time, those data will have to be exploited to the full. Deriving reliable estimates of rotational splitting from such data will be crucial for studying the dynamics of stars.

There are several possible sources of error in full-disc integrated data. Some are of a fundamental nature, and are unlikely to be affected by the method of analysis; others arise from the method of analysis, and the statistical model used for such analysis. An example of the former is the uncertainty associated with the stochastic nature of the excitation of the modes, which can lead to misidentification of components of a multiplet; it is sometimes referred to as *realization* noise. Another is the line blending at higher frequencies where the lines are broad, which renders it difficult, even impossible, to distinguish components of a multiplet, and can lead to systematic error. Of the latter, potential and neglected correlations between the $l+1$ (in the solar case) visible components of a multiplet can create systematic errors in a manner similar to that caused by the line blending. More broadly, any incorrect modelling of the profile and its statistics can lead to systematic error. Finally, even if appropriate modelling is used, inappropriate use of maximum-likelihood estimators (MLE) can also lead to systematically biased results; it is well known from information theory that MLE are typically unbiased only *asymptotically* as the amount of data tends to infinity (see Appourchaux, Gizon & Rabello-Soares 1998 for a review of the properties of MLE). Chang (1995) studied the systematic errors arising from the last four sources of error. He reported on how systematic errors in the splitting measurements of $l=1$ multiplets from whole-disc observations could arise from mode blending or mode correlations. Chaplin et al. (1998) reported also on similar findings using Monte-Carlo simulations. For higher-degree modes, it is expected that any systematic error should be lower than it is for $l=1$, because there are more components to assist the measurement, thereby increasing the degree of redundancy at given angular resolution. It is fortunate that for whole-disc observations the visibility functions are the greatest for the sectoral modes, which have the greatest influence in the determination of the mean multiplet splitting.

The purpose of this work is to assess the amount of systematic error that might arise in measuring the splitting for $l=1,2$ and 3. We adopt a simple theoretical model of full-disc integrated power spectra, and study its statistical properties. These properties are checked against real data to ensure that the model is realistic enough for our purpose. After validating the model, we carry out Monte-Carlo simulations for measuring the splitting. The simulation is performed with a set of parameters spanning different signal-to-noise ratios, linewidths and observing times. Although most observers fit the data using pair of modes (e.g. l=0-2, l=1-3), we have neglected this l-blending effect because the separation is an order of magnitude greater than the splitting. Therefore since we are concerned only with m-component blending, we simulate only one l at a time. We discuss the reason for the systematic error in the splitting so inferred, and how it could be reduced.

2 STATISTICS OF P-MODE MULTIPLET POWER SPECTRA

2.1 Theoretical model

For the purpose of generating artificial data, we model a set of intrinsically damped oscillators excited by a series of acoustic impulses imagined to have been produced by turbulent granules in the very thin outer superadiabatic boundary layer (immediately beneath the photosphere) of the solar convection zone, the time scale of each impulsive event being much shorter than the characteristic lifetime of the modes. It is convenient to express the signal $S(t)$ from a multiplet, comprising various azimuthal orders m, as a sum of the contributions from each event:

$$S(t) = \sum_k S_k(t) \ , \tag{1}$$

where $S_k(t)$ is the contribution of event k, and t is time. In our simple model, modes are excited locally at time t_k, at colatitude θ_k and azimuthal angle ϕ_k to amplitude a_k; the multiplet has mean frequency ω_0 and damping rate γ ($=\Gamma/2$, the half width at half maximum). The signal, integrated over the solar disc, is

$$\begin{aligned} S_k(t) \quad = \quad & \sum_m \alpha_m \cos[(\omega_0 + m\Omega)(t-t_k) + m\phi_k] \\ & \times P_l^m(\cos\theta_k) \times a_k e^{-\gamma(t-t_k)} H(t-t_k) \ , \end{aligned} \tag{2}$$

where P_l^m is an associated Legendre function, normalized such that

$$(1+\delta_{m,0}) \int_{-1}^{1} [P_l^m(\mu)]^2 \mathrm{d}\mu = 1 \ , \tag{3}$$

where $\delta_{m,n}$ is the Kronecker delta, and H denotes the Heaviside function. For simplicity we have assumed the m components to be separated by the constant spacing Ω, the rotational splitting. Again for simplicity, we assume that the points (θ_k, ϕ_k) are uniformly distributed on the sphere, and consequently components of the multiplet are on average excited to the same amplitude (see Chang & Gough 1998); however, the visibility coefficients α_m (which are normalized such that $\sum_m \alpha_m^2 = 1$) differ, for they depend on the geometry of the modes. We also ignore the initial rise time (the duration of the excitation) of $S_k(t)$, because it is assumed to be much shorter than the mode lifetime. Finally, we add noise $N(t)$, obtaining the observed signal

$$S_{\rm obs}(t) = S(t) + N(t) \ , \tag{4}$$

and we calculate the Fourier transform

$$F(\omega) \equiv \int_{-\infty}^{\infty} S_{\rm obs}(t) e^{-i\omega t} \mathrm{d}t \ . \tag{5}$$

By defining

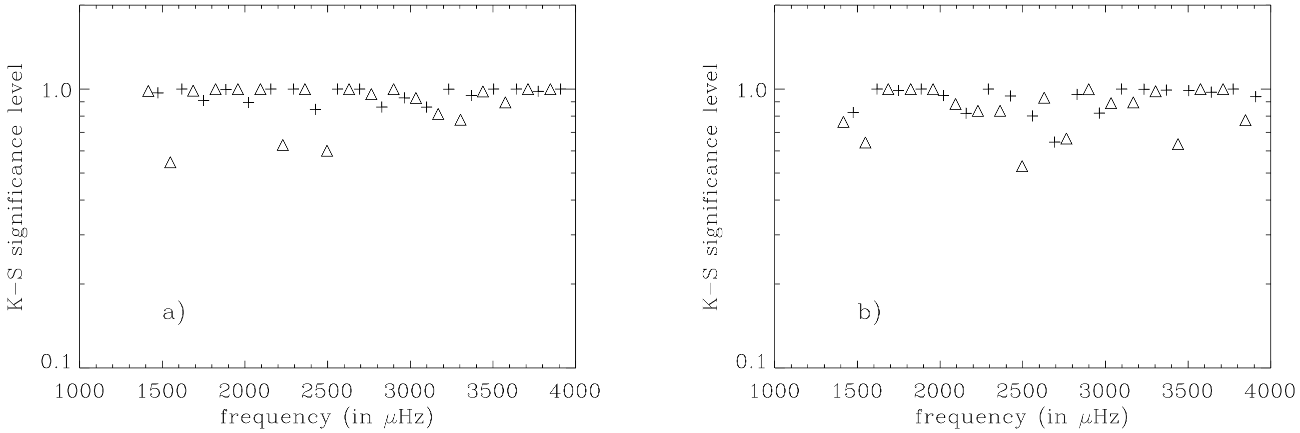

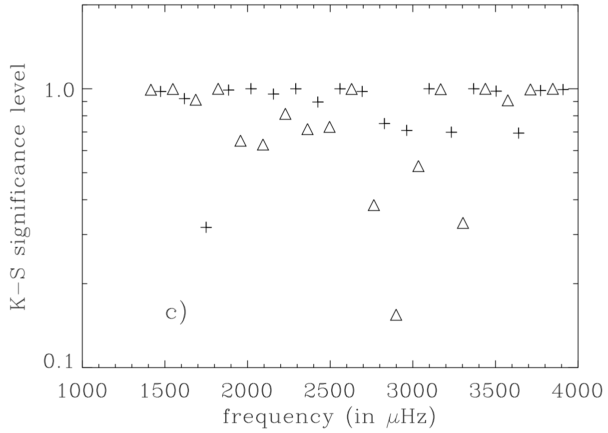

Figure 1. Kolmogorov-Smirnov tests for the GONG data: (a) for the real part of the Fourier spectra, (b) for the imaginary part of the Fourier spectra, (c) for the power spectra. The Fourier spectra were tested against a normal distribution, and the power spectra against a χ^2 with 2 dof distribution. The triangles and crosses represent the l = 0-2 and l = 1-3 pairs, respectively. The samples were taken from the fitting window of 28 μHz.

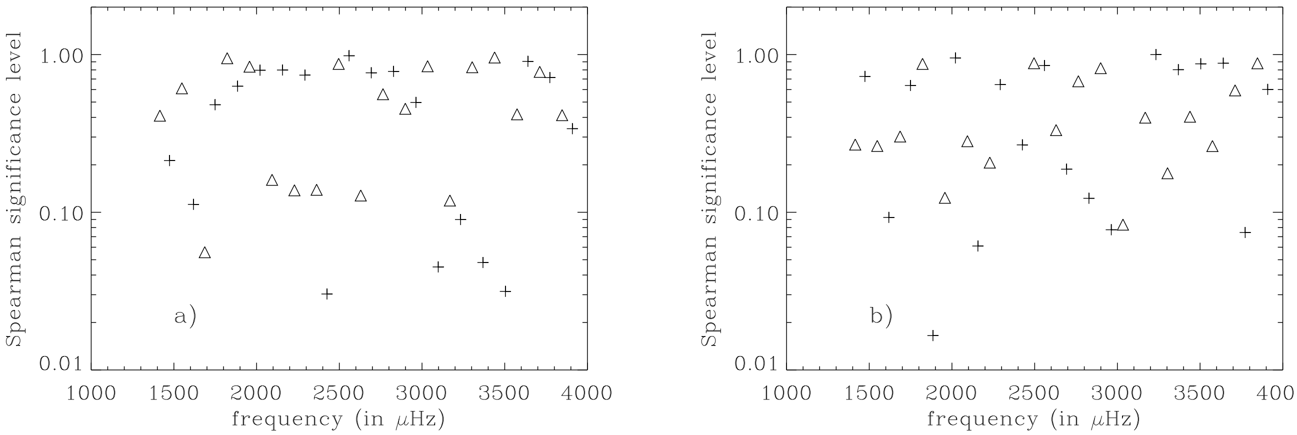

Figure 2. Spearman rank test for the GONG data: (a)for the adjacent frequency bins of the real part and (b) of the imaginary part of the Fourier spectra. The triangles and crosses represent the l = 0-2 and l = 1-3 pairs, respectively. The samples were taken from the fitting window of 28 μHz.

$$\xi_m(\omega) \equiv \sum_k a_{km} \cos(\omega t_k - m\phi_k), \tag{6}$$

and

$$\eta_m(\omega) \equiv \sum_k a_{km} \sin(\omega t_k - m\phi_k) \ , \tag{7}$$

where $a_{km} \equiv a_k P_l^m(\cos\theta_k)$, and denoting the real and imaginary parts of the Fourier component of $N(t)$ at frequency ω by $\zeta_{\rm r}(\omega)$ and $\zeta_{\rm i}(\omega)$, it is found, in the vicinity of ω_0, that

$$F(\omega) \simeq \frac{1}{2i} \sum_m \alpha_m \frac{\xi_m - i\eta_m}{\omega - \omega_0 - m\Omega - i\gamma} + \zeta_{\rm r} + i\zeta_{\rm i} \ . \tag{8}$$

Note that we have implicitly assumed that the sampling interval Δt is short enough and the observing time T is long enough to ensure that the formulae are applicable for simulating a discrete Fourier transform in the frequency range of our interest.

At each ω, the pair (ξ_m, η_m) correspond to the coordinates of a point undergoing a random walk in two dimen-

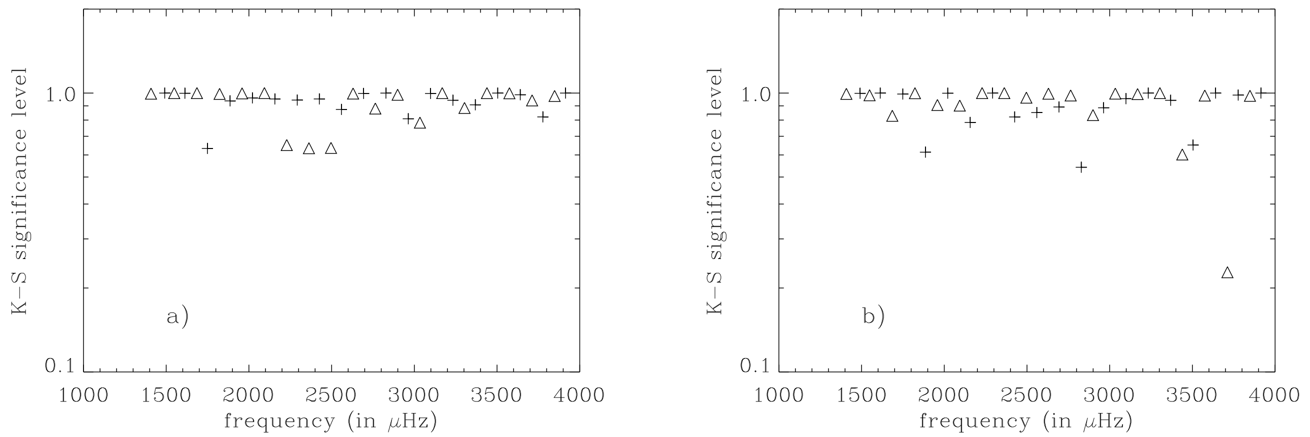

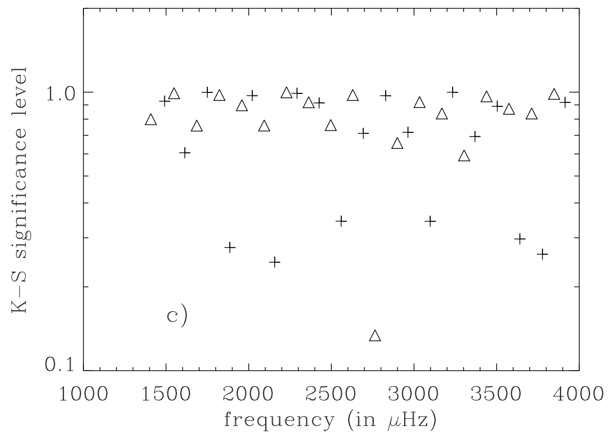

Figure 3. Kolmogorov-Smirnov tests for the LOI data: (a) for the real part of the Fourier spectra, (b) for the imaginary part of the Fourier spectra, (c) for the power spectra. The Fourier spectra were tested against a normal distribution, and the power spectra against a χ^2 with 2 dof distribution. The triangles and crosses represent the l = 0-2 and l = 1-3 pairs, respectively. The samples were taken from the fitting window of 28 μHz.

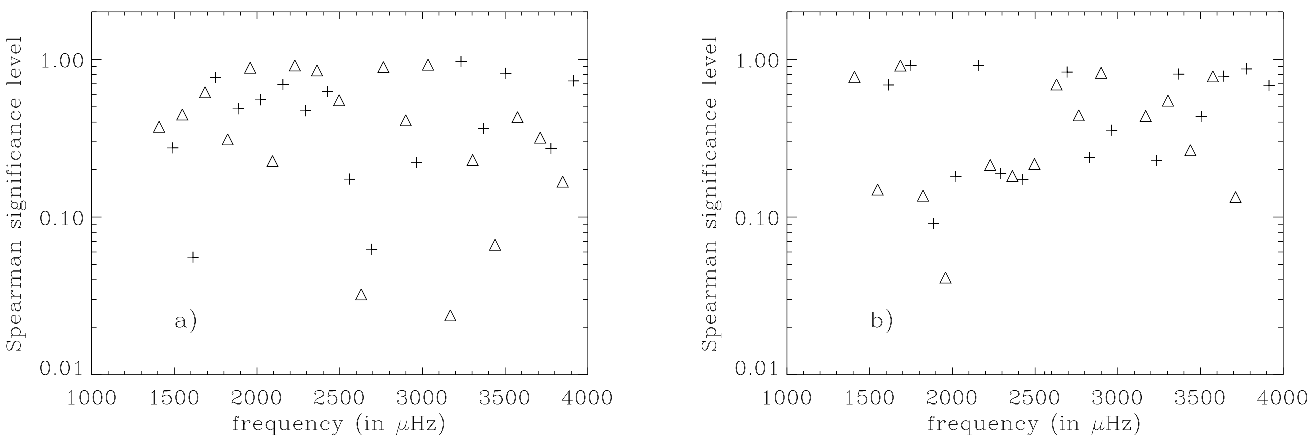

Figure 4. Spearman rank test for the LOI data: (a) for the adjacent frequency bins of the real part and (b) of the imaginary part of the Fourier spectra. The triangles and crosses represent the l = 0-2 and l = 1-3 pairs, respectively. The samples were taken from the fitting window of 28 μHz.

sions with varying step a_{km}, the two components being statistically independent. We assume the excitation events are Poisson distributed in time. Then the correlations between ξ_m and η_m at different frequencies ω and ω' satisfy

$$E[\xi_m(\omega)\xi_m(\omega')] = E[\xi_m^2(\omega)]\frac{\sin[(\omega-\omega')T]}{(\omega-\omega')T}\ , \qquad (9)$$

$$E[\eta_m(\omega)\eta_m(\omega')] = E[\eta_m^2(\omega)]\frac{\sin[(\omega-\omega')T]}{(\omega-\omega')T}\ , \qquad (10)$$

where $E[\cdots]$ denotes statistical average (expectation). In our simulation these correlations vanish because the Fourier components are created only in discrete bins, bin j being centred at $\Omega_j = 2\pi j/T$, and therefore for any pair of frequencies the difference $\omega - \omega'$ is a multiple of $2\pi/T$. Finally, for a sufficiently large number of excitation events, the two components are Gaussian distributed irrespective of the distribution of a_k (and hence a_{km}). As a result of all the above, ξ_m and η_m can be generated as independent sets of Gaussian random numbers in each frequency bin.

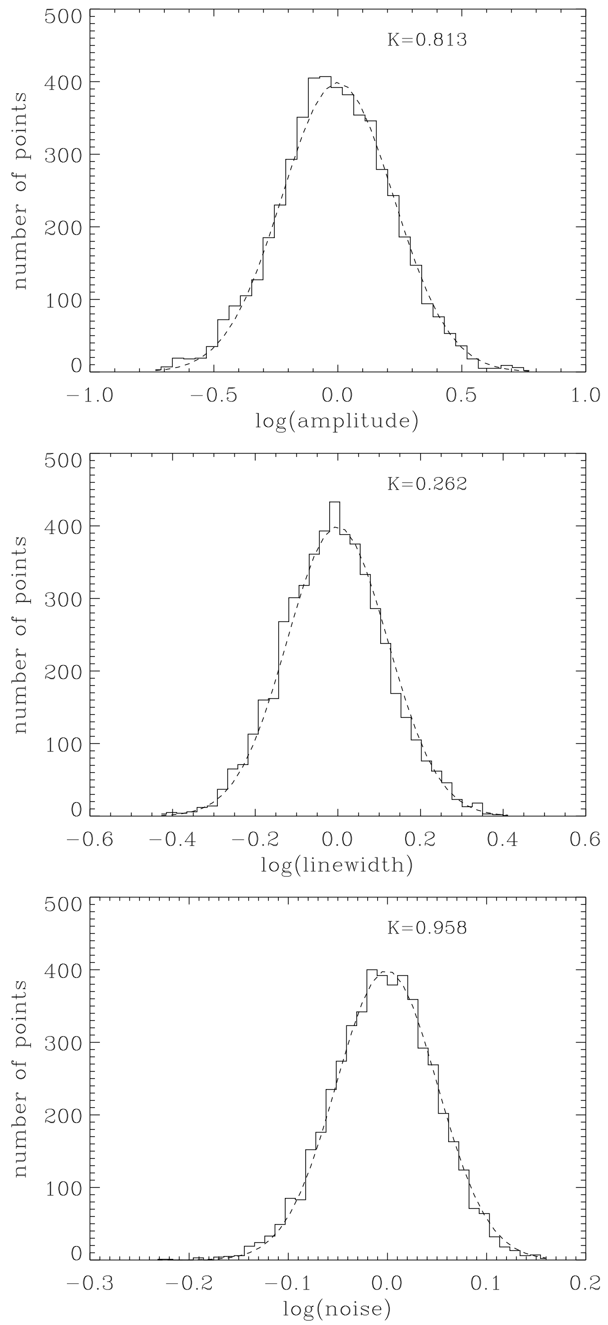

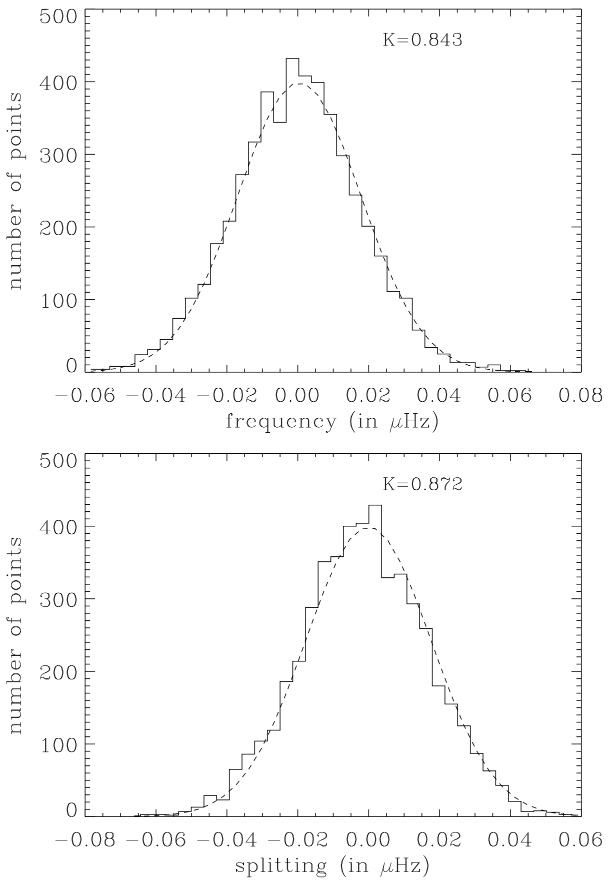

Figure 5. Histograms of 5000 realizations of the fitted parameters of an $l = 1$ multiplet: (top left) logarithm of inferred amplitude measured in units of the input amplitude, (top right) difference between the inferred multiplet frequency and the input value, (middle left) logarithm of inferred linewidth in units of the input linewidth, (middle right) difference between the inferred and the input splitting, (bottom left) logarithm of the inferred rms noise in units of the input value. The input parameters were the following: 100 (amplitude), 0.1 μHz (frequency), 0.25 μHz (linewidth), 0.4 μHz (splitting), 0.1 (noise). The dashed curves are Gaussians whose means and variances are the sample means and the sample variances. The bin sizes are one fifth of the appropriate standard deviations. The time series is 660 days long. K is the probability of a deviation from expectation larger than observed, as measured by the Kolmogorov-Smirnov test.

Since the noise components $\zeta_{\rm r}$ and $\zeta_{\rm i}$ are also assumed to be independently Gaussian distributed, the real part and the imaginary part of $F(\omega)$ are both independently Gaussian distributed. Consequently the distribution of power $P(\omega) = |F(\omega)|^2$ is χ^2 with two degrees of freedom (2 dof) with an expectation $P_0(\omega)$ determined as follows:

$$P_0(\omega) = A \sum_m \frac{\alpha_m^2}{(\omega - \omega_0 - m\Omega)^2 + \gamma^2} + B \ , \tag{11}$$

where

$$A = \frac{1}{4} \sum_k E[a_{km}^2] \tag{12}$$

and B is the amplitude of the background noise. The amplitude A does not depend on m because of our assumption concerning the distribution of (θ_k, ϕ_k).

It is worth noting that the real and imaginary parts of $F(\omega)$, namely $F_{\rm r}$ and $F_{\rm i}$, satisfy

$$\lim_{T\to\infty} E[F_{\rm r}(\omega)F_{\rm r}(\omega')] \quad = \quad E[F_{\rm r}^2(\omega)]\delta(\omega - \omega'), \tag{13}$$

$$\lim_{T\to\infty} E[F_{\rm i}(\omega)F_{\rm i}(\omega')] \quad = \quad E[F_{\rm i}^2(\omega)]\delta(\omega - \omega') \tag{14}$$

under assumptions that are reasonable but broader than those required for deriving equations (8) and (9) (cf. Davenport & Root 1958, Gabriel 1994). This adds support for using independent Gaussians for simulating sufficiently long time series. In the next subsection, by examining real solar

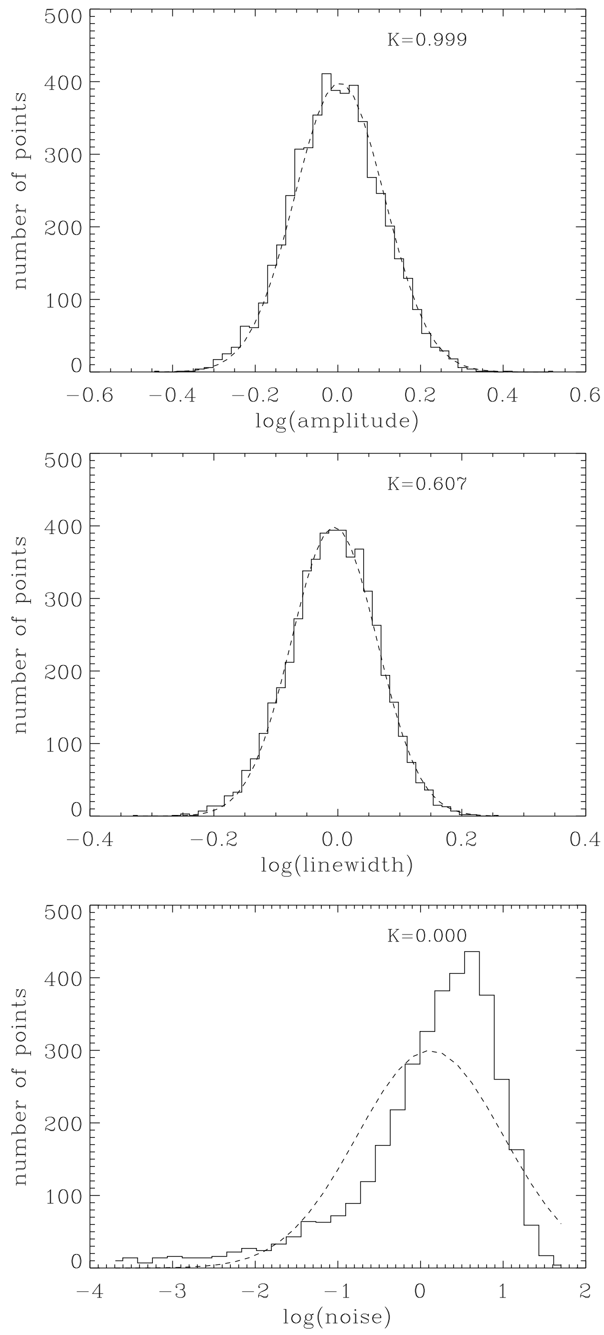

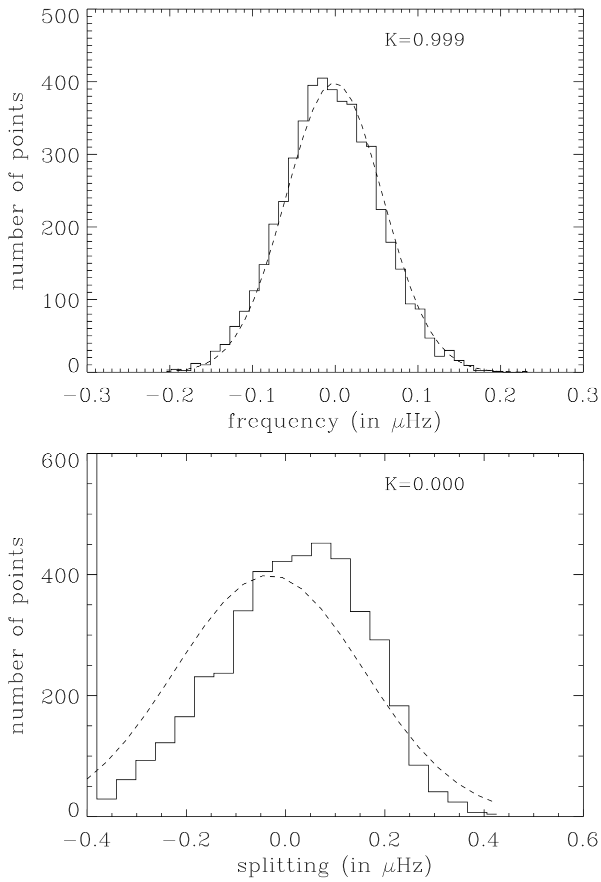

Figure 6. Histograms of 5000 realizations of the fitted parameters of an $l = 1$ multiplet as in Fig. 5. The input parameters were the following: 100 (amplitude), 0.1 μHz (frequency), 2.00 μHz (linewidth), 0.4 μHz (splitting), 0.1 (noise). The bin sizes are one fifth of the appropriate standard deviations. The time series is 660 days long. K is the probability of a deviation from expectation larger than observed, as measured by the Kolmogorov-Smirnov test. In the histogram for the frequency splitting there are 597 null values (out of the 5000 plotted data); the mean of the inferred deviations of the splittings from Ω is -0.033 μHz if those null values are included, $+0.017$ μHz if they are ignored. Please note that 1200 estimations of the noise produced values lower than the range accommodated by the window in the figure; these low values arise from the inability of our fitting procedure to detect the noise when the linewidth is large and the signal-to-noise ratio is high.

data, we address how realistic these statistical properties of our model are.

2.2 Real data

The model described above is used in most cases for fitting full-disc integrated data. In this section we describe the test we carried out on real solar data to verify the validity of the model. We used 1080 days of GONG data and 784 days of LOI data (Hill et al. 1996; Appourchaux et al. 1997). Both data sets were obtained from imaging instruments, and we used the $l = 0$ signal as a proxy for full-disc integrated data. The signal is only a proxy because the pixels do not cover the entire solar disc. The duty cycle was 84% for the GONG data and 99% for the LOI data. In the GONG data the first temporal alias has an amplitude of about 5% in the Fourier spectrum, yielding 0.25% in the power spectrum. We tested the following hypotheses:

H1: the real and imaginary parts of the Fourier spectra are Gaussian distributed;
H2: the power spectrum has χ^2 with 2 dof statistics;
H3: data from adjacent frequency bins are independent of each other.

The first two hypotheses were tested using a Kolmogorov-Smirnov (K-S) test, and the third was tested using a Spearman rank test (e.g. Press et al. 1986). Since we do not have many realizations of a given profile (for long-time series, at least) we cannot perform an ensemble average;

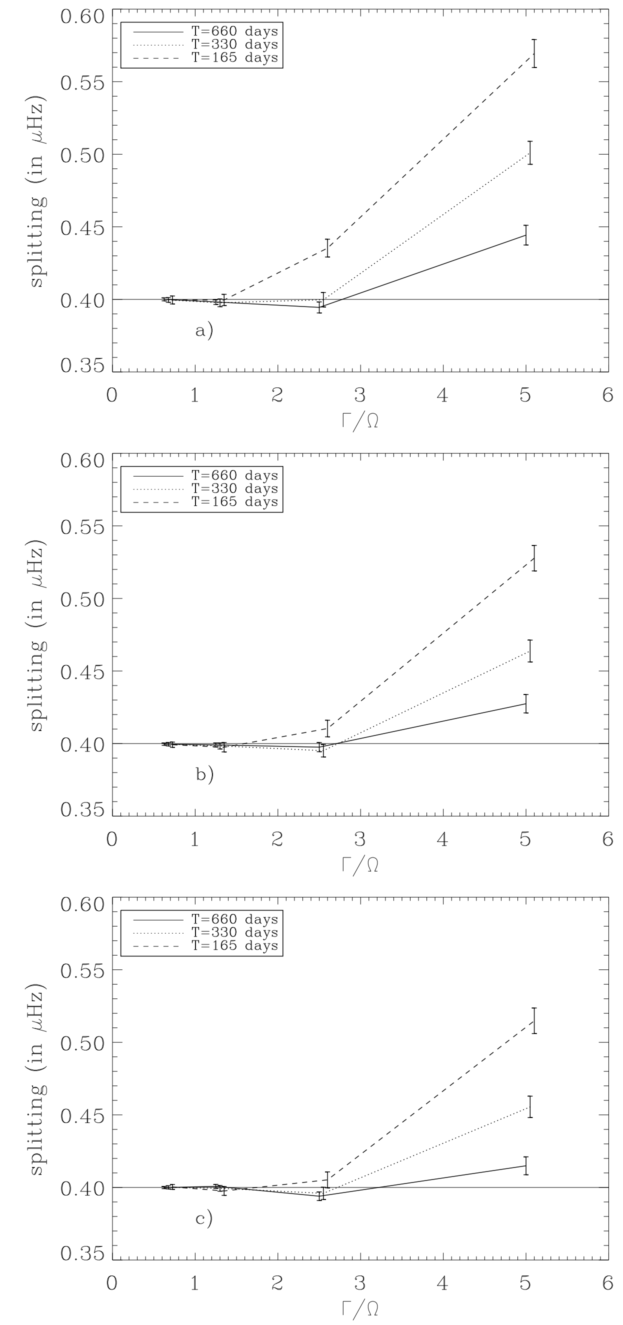

Figure 7. Fitted splitting as a function of the inverse of the reduced splitting (ratio of splitting Ω to linewidth Γ) for l = 1 for various lengths of time series and the following signal-to-noise ratios: (a)10, (b) 100, (c) 1000. The error bars denote ± 3 standard deviations from the mean of the inferred splitting.

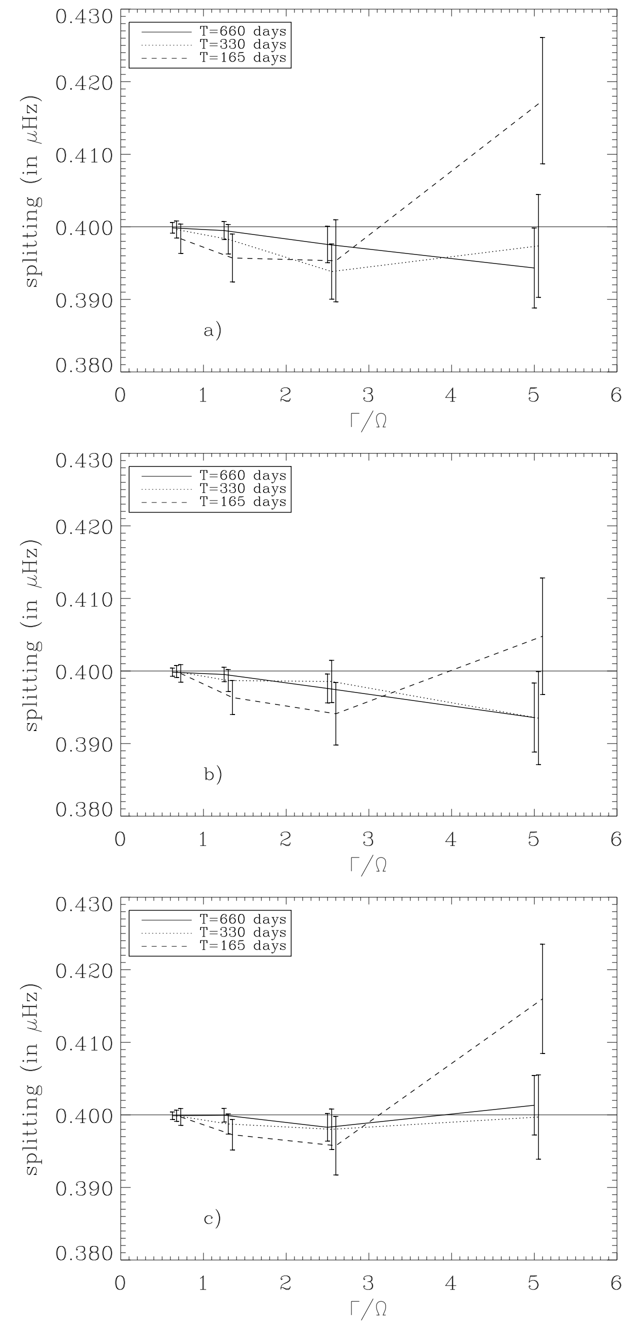

Figure 8. Fitted splitting as a function of the inverse of the reduced splitting (ratio of splitting Ω to linewidth Γ) for l = 2 for various lengths of time series and the following signal-to-noise ratios: (a) 10, (b) 100, (c) 1000. The error bars denote ± 3 standard deviations from the mean of the inferred splitting.

therefore we decided to use the set of numerous data bins for the test. For these to be substituted for an ensemble, the signal has to be rescaled so that it has a uniform variance over the frequency bins (otherwise the sample over the bins would not resemble the sample over realizations). Accordingly we applied the following sequence of procedures:

(i) fit the power spectrum over the frequency range of 28 μHz assuming the statistics to be χ^2 with 2 dof with independent frequency bins;

(ii) divide each Fourier component by the square root of the fitted variance;

(iii) carry out a K-S test for the distribution of each Fourier component (normal distribution) and of the power spectrum (χ^2 distribution with 2 dof);

(iv) perform the Spearman rank test on pairs of the Fourier components in adjacent bins.

We fit the l=0-2 pairs with 7 independent parameters (two amplitudes, two frequencies, common linewidth, background

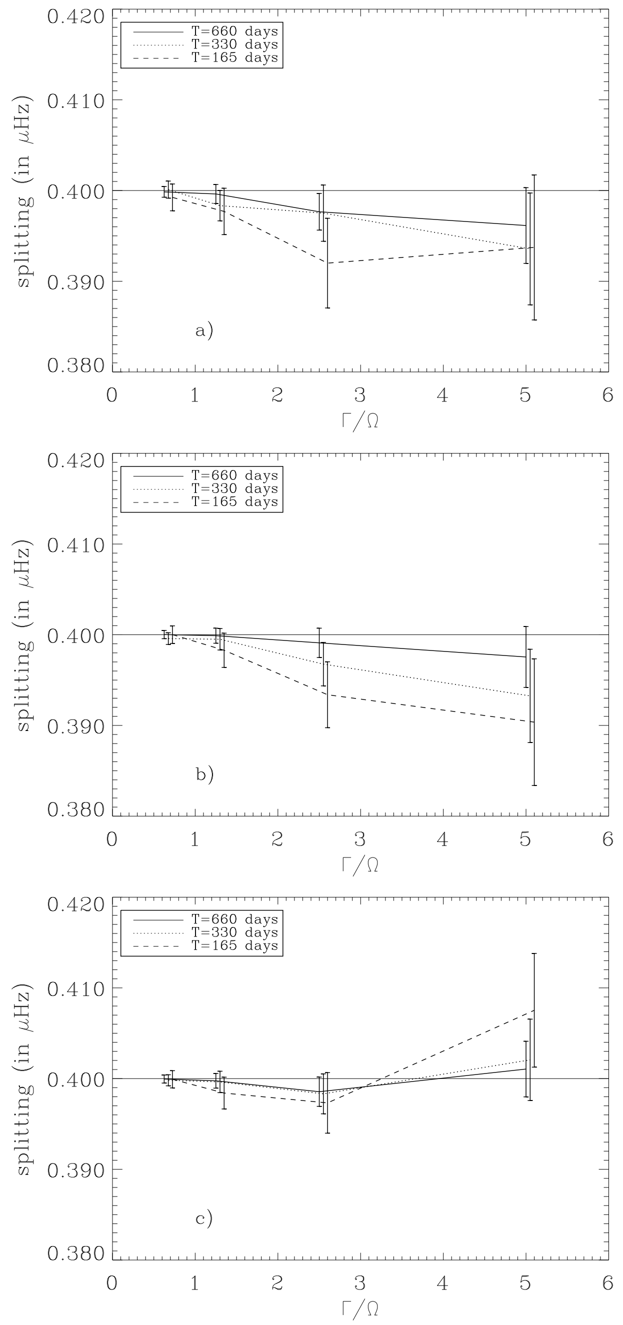

Figure 9. Fitted splitting as a function of the inverse of the reduced splitting (ratio of splitting Ω to linewidth Γ) for $l = 3$ for various lengths of time series and the following signal-to-noise ratios: (a) 10, (b) 100, (c) 1000. The error bars denote ± 3 standard deviations from the mean of the inferred splitting.

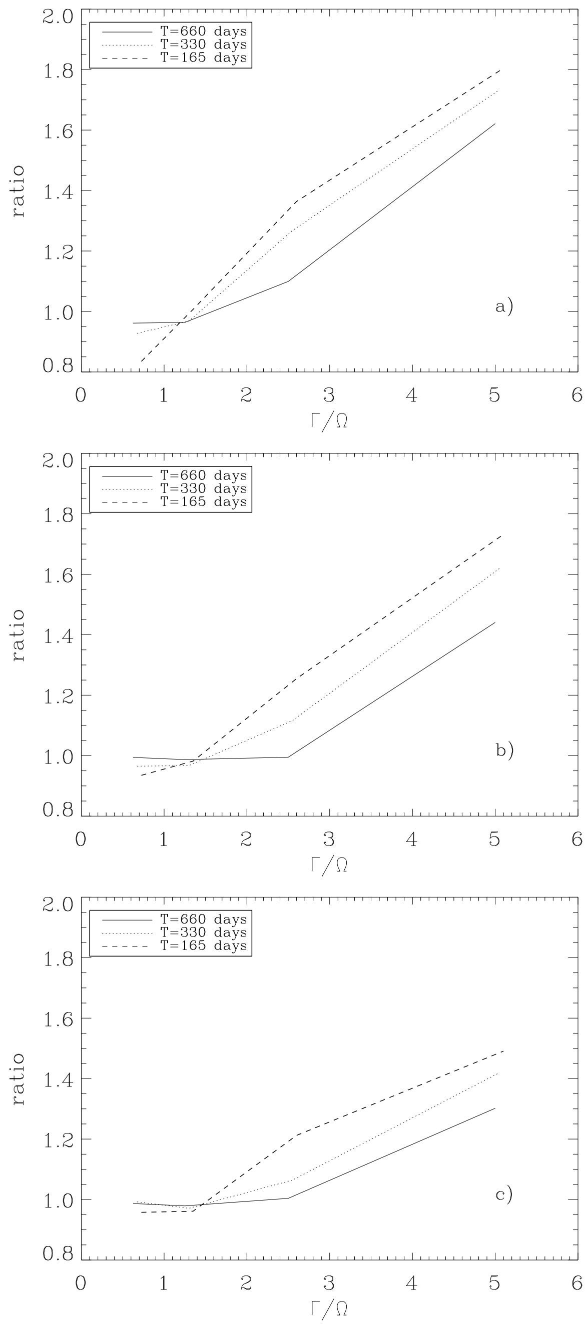

Figure 10. Ratio of splitting error bars to splitting standard deviation as a function of the inverse of the reduced splitting (ratio of splitting Ω to linewidth Γ) for $l = 1$ for various lengths of time series and the following signal-to-noise ratios (a) 10, (b) 100, (c) 1000. The splitting error bars are an average of the error bars derived for each realization; it is an estimate of the typical error bar for a single realization. The splitting standard deviation is derived from the scatter of the fitted splittings.

noise, splitting). The l=1-3 pairs are similarly fitted but with one additional splitting (8 parameters). The temporal side-lobes for GONG were not taken into account.

In both tests, we quantify how far a sample deviates from the properties expected from the tested hypothesis, and calculate the probability of a deviation as large as or greater than that observed (significance level). Figures 1 and 3 show the results of the K-S test: we cannot reject the hypothesis that the GONG and LOI Fourier spectra are not Gaussian distributed, or that their power spectra are not distributed as χ^2 with 2 dof. Figures 2 and 4 show the results of the Spearman rank test: for both the GONG and the LOI data the hypothesis of non-correlation is accepted with 99% confidence level (Spearman rank test returns significance level higher than 0.01). To have some idea about the actual level of correlation, we have calculated the correlation in a sample

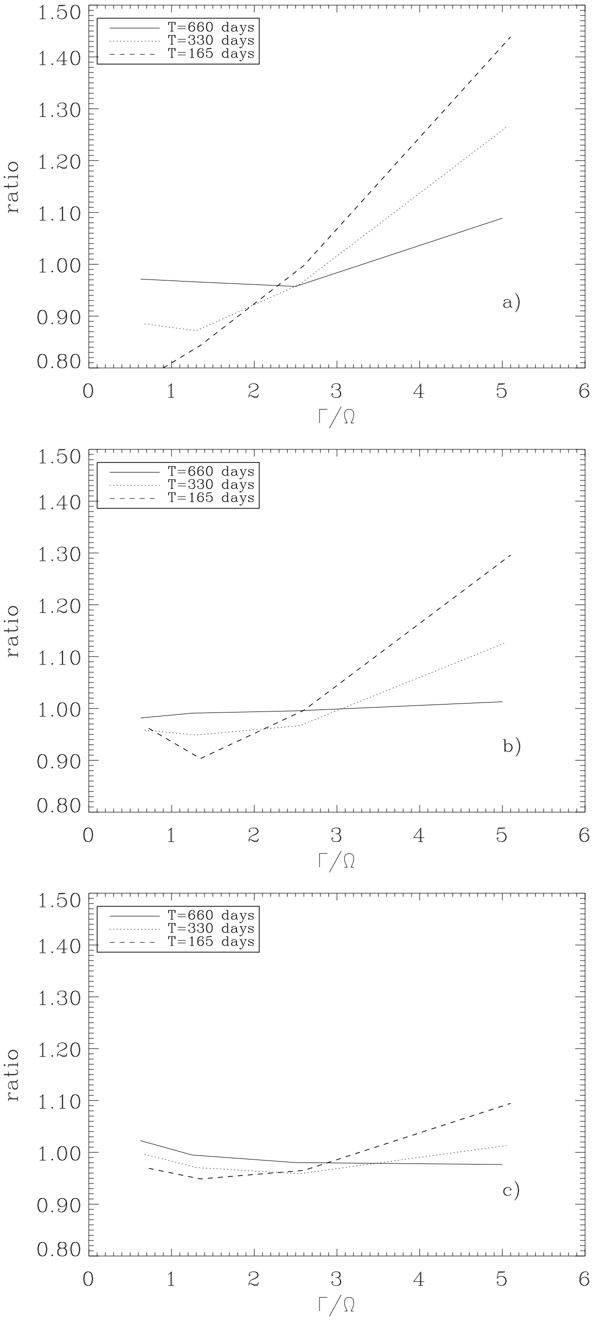

Figure 11. Ratio of splitting error bars to splitting standard deviation as a function of the inverse of the reduced splitting (ratio of splitting Ω to linewidth Γ) for $l = 2$ for various lengths of time series and the following signal-to-noise ratios (a) 10, (b) 100, (c) 1000. The splitting error bars are an average of the error bars derived for each realization; it is an estimate of the typical error bar for a single realization. The splitting standard deviation is derived from the scatter of the fitted splittings.

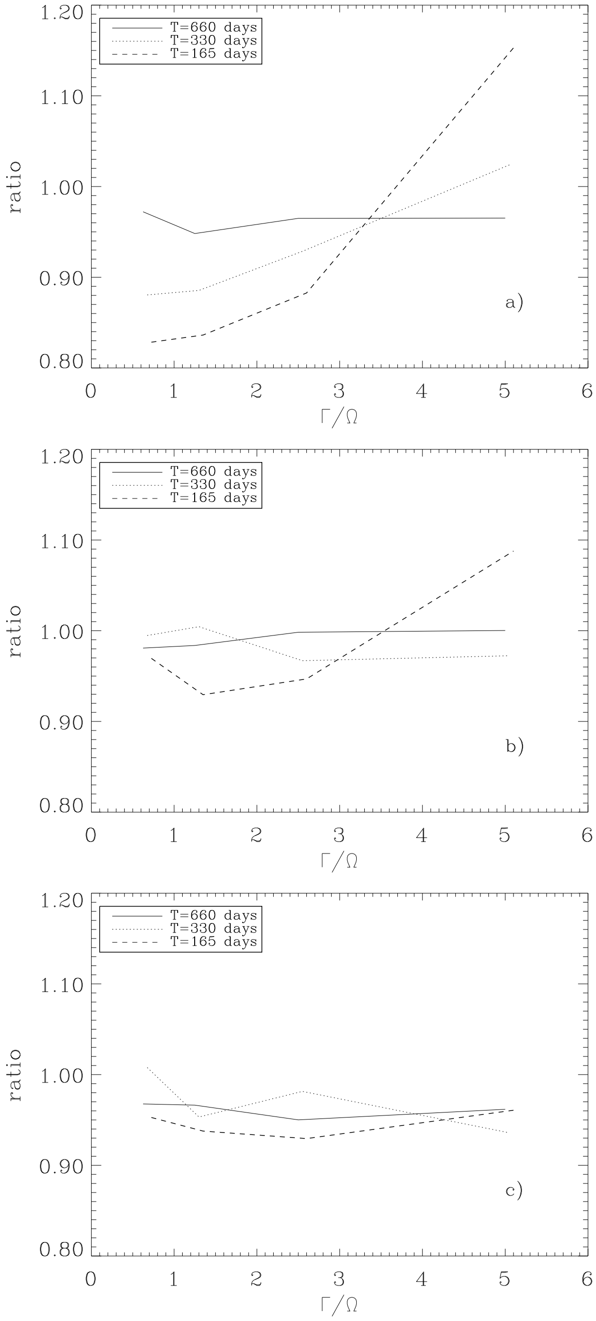

Figure 12. Ratio of splitting error bars to splitting standard deviation as a function of the inverse of the reduced splitting (ratio of splitting Ω to linewidth Γ) for $l = 3$ for various lengths of time series and the following signal-to-noise ratios (a) 10, (b) 100, (c) 1000. The splitting error bars are an average of the error bars derived for each realization; it is an estimate of the typical error bar for a single realization. The splitting standard deviation is derived from the scatter of the fitted splittings.

for which the expectation of the significance level would be 0.01. This depends on the size of the sample; for the GONG data the correlation coefficient would be 6%, and for the LOI data, 7%.

We can safely conclude that the approximation of having independent frequency bins is indeed valid. It is worth noting that this approximation applies to the GONG data even though the duty cycle is as low as 84%. These tests validate the assumptions that are usually made when fitting Fourier or power spectra in helioseismology. It also justifies all the Monte-Carlo simulations carried out under the same set of assumptions for the purpose of understanding the parameters returned by the fitting procedures.

3 MONTE-CARLO SIMULATION

Monte-Carlo simulations have become an essential tool for understanding the process of fitting helioseismic data. They are performed routinely to understand the various problems associated with MLE (e.g. Chaplin et al. 1997; Appourchaux et al. 1998). As stated above, the statistical distribution of the power spectra for full-disc integrated data is χ^2 with 2 degrees of freedom. For $l=2$ and 3, we have assumed in our simulations that the expectation of the squared amplitude ratio (resulting from the different visibility coefficients) between the $m=l-2$ mode and the $m=l$ mode is 0.65 in the power spectra ($\alpha_{l-2}^2/\alpha_l^2=0.65$); this ratio is taken for intensity measurements such as those performed by VIRGO. We have carried out simulations with the following parameter sets:

(i) 3 signal-to-noise ratios (A/B): 1000, 100, 10,
(ii) 4 linewidths (Γ): 2μHz, 1μHz, 0.5μHz, 0.25μHz,
(iii) 3 observation times (T): 165 days, 330 days, 660 days.

The rotational splitting Ω was 0.4μHz in all cases. The maximum signal-to-noise ratio obtained by the LOI and full-disc integrated GONG is about 50 and 100, respectively. Our range of signal-to-noise ratios represent what is typically found with helioseismic instruments. The smallest linewidth (0.25 μHz) corresponds to a mode at a frequency around 1800 μHz, while that of the largest linewidth corresponds to 3400 μHz.

We generated an artificial power spectrum for each multiplet separately, and then we fitted the function $P_0(\omega)$ to it using a window size of 28μHz. We used the MLE, fitting 5 parameters, namely amplitude A, linewidth Γ, frequency ω_0, splitting Ω and background noise level B to each profile. Powell's method (e.g. Press et al. 1986) was used to maximize the likelihood function. The simulations were performed for $l=1,2$ and 3. Note that the amplitudes of each of the m components in the formula (2.1) for $P_0(\omega)$ are the same, aside from the weighting by the known visibility coefficients α_m^2. Assuming otherwise would have introduced an additional systematic error in the splitting determination (Appourchaux et al. 1998; Chang, Gough & Sekii 1998). We performed 5000, 2500 and 1500 simulations for $l=1,2$ and 3 respectively; the decreasing number of simulations with l is to take account of the increasing precision as l increases (see later in this section).

In almost all cases tested, the averages of the fitted parameters agree with the input parameters within 3σ. The exceptions are the splitting and, to a lesser extent, the noise level.

Figure 5 shows histograms of the fitted parameters (amplitude, linewidth, frequency, splitting and noise). The amplitude, frequency and linewidth have Gaussian distributions. The noise has a Gaussian distribution when the signal-to-noise ratio is low. The splitting has a Gaussian distribution when the linewidth is narrow or the observation time is long. Figure 6 shows histograms when the linewidth is large (2 μHz). The noise histogram of Figure 6 is typical when the signal-to-noise ratio is high. In this figure the splitting histogram has a large number (597) of null values; such a situation arises whenever the linewidth is large or the time series is short. The presence of inferred null splitting then distorts the histogram, and the fitted splittings do not follow a Gaussian distribution as they do in Figure 5.

This behaviour of the histograms adds a complication to the process of deriving meaningful splitting frequencies. If the zeros are included in the averaging process (as was the case in fitting the Gaussians illustrated by dashed curves in Figures 5 and 6), the average splitting is systematically lower than the input splitting. With real data, however, observers do explicitly reject the null splitting, partly because the inferences are associated with large estimated errors (as shown by Toutain & Appourchaux 1994). For computing a 'realistic' estimate of the splitting from the histograms, we therefore chose also to exclude the null splittings. Figures 7 to 9 show such estimates of average splitting for $l=1,2$ and 3. It is clear that on the whole the splitting is positively biased when $l=1$. For $l>1$ the amount of systematic error is not significantly different from zero.

Figure 6 suggests that if one could 'put back' all the null estimates of the splitting into the main part of the distribution the systematic error might at least be reduced. If these null cases actually correspond to local minima found at zero splitting, with a global minimum closer to the input splitting of 0.4μHz, or alternatively to a (weak) global minimum at zero but with a local minimum close to 0.4μHz, there is a chance of avoiding these null cases by adding a penalty function to the likelihood function. In every example we have examined, however, that is not the case: the maximum of the likelihood function does indeed occur at the zero, and there is no hint of even a local maximum very close to 0.4μHz.

It must be pointed out that for very high signal-to-noise ratio (≈ 1000) and very large linewidth the determination of the noise is unreliable (see Figure 6). This is particularly evident from the existence of the large number of estimates that are too low to include in the figure. In our simulation the data with very low noise estimates are included in the estimates of the frequency splitting. Not to do so is likely to increase the bias. For example, had the data with estimated noise levels too low to accommodate in the range of the histogram in Figure 6 been excluded from the analysis, the splitting would have been overestimated by 20 nHz. Evidently the fitting strategy plays an important role in determining the amount of the bias, especially for $l=1$ (bottom panel of Fig 7).

Fortunately, the systematic error is reduced when the duration T of the observation is greater, or when the linewidth is smaller, or when the signal-to-noise ratio is higher. Moreover, the systematic error becomes smaller as l increases, roughly as the inverse of l^3, and becomes significantly smaller than the random error, which scales as the inverse of the square root of

$$\sum_{m=-l,l,2} m^2 = \frac{l(l+1)(l+2)}{3} \; . \tag{15}$$

This formula is derived (after Toutain & Appourchaux 1994) for full-disc integrating instruments assuming the splitting-to-linewidth ratio to be large. A similar formula for imaging instruments was derived by Veitzer, Tomczyk & Schou (1993). In our case, the relative ratio of systematic error to formal (random) error is 1.414, 0.353 and 0.166, for $l=1,2$ and 3, respectively.

Figures 10 to 12 show the comparison between the error bars derived for a single realization and the splitting standard deviation derived from the scatter in the estimated splittings. If the error bars derived for a single realization are meaningful, the ratio should be close to unity; this is the case when the linewidth is narrow or when the time series is long. When that is not the case, the error bars derived overestimate the true standard deviation. This is a better situation than underestimating the deviation; it gives a smaller weight to the associated splitting, thereby reducing slightly the systematic error associated with the splitting derived for a single power-spectrum realization.

4 DISCUSSION

The histograms of the inferred frequency splitting recomputed excluding all null splittings are closer to normal distributions than are those in which all the splittings are included, but they still cannot be considered to be Gaussian. Again with real data, observers sometimes compute a degree-by-degree 'mean' splitting using weighted averages to minimize the variance. In this averaging it is explicitly assumed that the random variables observed are all Gaussian distributed. This is in contradiction to our result from Monte-Carlo simulations: the splittings derived for large linewidths or short time series are *not* Gaussian distributed. There is a serious implication for inversion procedures, in which it is usually assumed, for lack of another obvious choice, that the errors in the splitting measurements are Gaussian distributed. Knowing that the statistics of the measurement errors are not Gaussian, but knowing little else about the distributions, perhaps explains to some degree why some observers do not disclose (or fit) their splittings above a certain linewidth (e.g. Lazrek et al. 1997). Of the two important classes of inversion methods (see, for example, Sekii 1997), the regularized least-squares fitting more directly depends on the assumption of errors being Gaussian distributed, at least in its formalism, since it *is* a maximum-likelihood fitting, with a penalty term which depends explicitly on the assumption of the statistics of the measurement errors. In the standard formulation of optimally localized averaging, the principal issue is how well the variance of a linear combination of the splittings is represented by the corresponding weighted sum of the variances of the splittings; with often thousands of the terms present, the outcome in this case is likely to be acceptable.

In some cases Monte-Carlo simulations of the kind we have carried out could be used to calibrate the estimate, so that the systematic error can be removed or reduced from the estimate. The simplest example of such a procedure is to decide the likely range of linewidth and signal-to-noise ratio, and then from Figs 7 to 9 decide in what range the amount of overestimation is likely to be (Chang 1995). Although this is a step forward, it would still give only a rough idea of Ω.

Let us consider how the procedure might be improved, by starting from a simple example. Let us assume, first, that all the quantities other than the splitting Ω are precisely determined and yet the estimate $\Omega_{\rm MLE}$ obtained by MLE is biased. ¿From a Monte-Carlo simulation we know the probability distribution function of $\Omega_{\rm MLE}$, for given Ω: namely $\psi_1(\Omega_{\rm MLE};\Omega)$. In an ideal case this probability distribution function has a single δ-function ridge along $\Omega_{\rm MLE} = f(\Omega)$, where the function f is monotonic: $\psi_1(\Omega_{\rm MLE};\Omega) = \delta(\Omega_{\rm MLE} - f(\Omega))$. In this case, a precise calibration of the MLE is possible; for an estimate $\Omega^*_{\rm MLE}$ obtained by MLE, we infer that the real value is $\Omega^* = f^{-1}(\Omega^*_{\rm MLE})$.

If the ridge has finite width, then a precise calibration is no longer possible. But if the ridge is well defined, what is often done is to pretend that the ridge is very sharp, and repeat the above procedure. This corresponds to maximizing $\psi_1(\Omega^*_{\rm MLE};\Omega)$ over Ω to find the improved estimate Ω^*, and in fact this procedure is itself an MLE procedure, because $\psi_1(\Omega_{\rm MLE};\Omega)$ gives the (density of the) likelihood of Ω.

Having appreciated the above, let us consider a slightly more realistic case, in which we have also to take the effect of measurement error on the linewidth determination into account: the linewidth Γ and its MLE value $\Gamma_{\rm MLE}$ are distinguished (all the other variables are still assumed to have been satisfactorily determined). Again, from a Monte-Carlo simulation we know the joint probability distribution function $\psi_2(\Omega_{\rm MLE},\Gamma_{\rm MLE};\Omega,\Gamma)$. As a natural generalization of the previous case, for a set of estimates ($\Omega^*_{\rm MLE}$, $\Gamma^*_{\rm MLE}$) we can maximize $\psi_2(\Omega^*_{\rm MLE},\Gamma^*_{\rm MLE};\Omega,\Gamma)$ over Ω and Γ for an improved set of estimates.

Generally, this may yield better estimates. In our case, however, there is a danger of finding the maximum at $\Omega = \Omega_{\rm MLE}$ and $\Gamma =$ some small value, leading to no improvement. A detailed investigation is currently under way.

Another alternative would be to devise an unbiased splitting estimator in a more general way. One such approach was used by Quenouille (1956) to get unbiased estimators from MLE; this technique is yet to be applied in helioseismology or asteroseismology. However, the mere reduction of bias is not the be-all and end-all of the analysis; it is not desirable to reduce bias at the expense of an excessive increase in the magnitudes of the errors.

In stellar cases, another complication arises because of the (a priori) lack of knowledge of the inclination of the rotation axis with respect to the line-of-sight. This means that one would have to fit α_m at the same time, possibly increasing the systematic error.

5 CONCLUSIONS

We have shown that the splitting obtained by using MLE applied to full-disc integrated power spectra is positively biased for $l = 1, 2$. For example, for $l = 1$ with linewidth comparable to rotational splitting and a signal-to-noise ratio of 100, on average the splitting is overestimated by about 10% for a 165-day time series.

We suspect that not only is this bias the reason for the disparate inferences of rotational splitting that have been drawn from analyses of data from different instruments, as we mentioned in the introduction, but also that the greater linewidths at solar maximum (e.g. Chaplin et al. 1999), and consequently greater bias, has possibly led to an erroneous conclusion from data from a single instrument concerning a purported solar-cycle variation of the angular velocity of the solar core (Jiménez et al. 1994). To sustain this hypothesis, we have performed Monte-Carlo simulations for a 30-day observation time for a dipole mode with a 1-μHz linewidth and various signal-to-noise ratios. To simulate the solar-cycle variation, we applied an increase of 24% to the linewidths, as measured by Chaplin et al. (1999), without changing the frequency splitting Ω. The increase in the splitting estimated from our simulations ranged from 50 to 70 nHz, depending on the signal-to-noise ratio. This increase is about the same as that reported by Jiménez et al. (1994). In addition, the error bars could have been systematically underestimated, as they are smaller than what information theory would predict (Toutain & Appourchaux 1994). Therefore, a solar-cycle dependence of the angular velocity of the solar core is yet to be demonstrated.

For a given linewidth and signal-to-noise ratio, the systematic error is almost inversely proportional to the observing time. For a given observing time, the systematic error decreases in proportion to the inverse signal-to-noise ratio and increases in proportion to the linewidth. For modes of higher degree, the systematic error is smaller, and scales as l^{-3}. We note that because the (positive) bias of the inferred values of the frequency splitting increases as l decreases, and hence as the radius of the inner turning point of the mode decreases, ignoring that bias leads to an exaggerated estimate of the angular velocity of the solar core relative to its surroundings.

We have discussed means of deriving unbiased splitting estimators, but we have not ascertained the optimum procedure.

ACKNOWLEDGMENTS

LOI is an instrument of the VIRGO investigation on SOHO, which is a mission of international collaboration between ESA and NASA. The work reported here utilizes data obtained by the Global Oscillation Network Group (GONG) project managed by the National Solar Observatory, a Division of the National Optical Astronomy Observatories, which is operated by AURA, Inc. under a cooperative agreement with the National Science Foundation. The GONG data were acquired by instruments operated by the Big Bear Solar Observatory, High Altitude Observatory, Learmonth Solar Observatory, Udaipur Solar Observatory, Instituto de Astrofísico de Canarias and Cerro Tololo Interamerican Observatory. TS is grateful for the support by the Particle Physics and Astronomy Research Council. We are grateful to our referee, W.Chaplin, for his useful comments and for the quality of his reporting.

REFERENCES

Appourchaux, T. 1998, Proceedings of the SOHO6/GONG'98 workshop, in *Structure and Dynamics of the Interior of the Sun and Sun-like Stars*, Boston, USA, ESA SP-418, p. 37

Appourchaux, T., Toutain, T., Telljohann, U., Jimenez, A., Rabello-Soares, M. C., Andersen, B. N. & Jones, A. R. 1995, A&A, 294, L13

Appourchaux, T., Andersen, B. N., Fröhlich, C., Jimenez, A., Telljohann, U., & Wehrli, C. 1997, Sol. Phys., 170, 27

Appourchaux, T., Gizon, L., & Rabello-Soares, M.-C. 1998, A&A Sup. Series, 132, 107

Appourchaux, T., Gough, D.O., Sekii, T. & Toutain, T., 1998, in *Sounding Solar and Stellar Interiors*, eds. G. Berthomieu, J. Provost and F.X. Schmider (Observatoire de la Côte d'Azur), 3

Baglin, A. & The Corot Team 1998, in *New Eyes to See Inside the Sun and Stars*, eds F.-L. Deubner et al. , IAU Symposium 185, 301

Chang, H-Y. 1995, Ph.D. Dissertation (University of Cambridge)

Chang, H-Y., Gough, D.O., 1998. Sol. Phys., 181, 251

Chang, H-Y., Gough, D.O., Sekii, T., 1998, in *Sounding Solar and Stellar Interiors*, eds. G. Berthomieu, J. Provost and F-X. Schmider (Observatoire de la Côte d'Azur), 13

Chaplin, W. J., Elsworth, Y., Howe, R., Isaak, G. R., McLeod, C. P., Miller, B. A.,& New, R. 1996, MNRAS, 280, 849

Chaplin, W. J., Elsworth, Y., Howe, R., Isaak, G. R., McLeod, C. P., Miller, B. A. & New, R. 1997, MNRAS, 287, 51

Chaplin, W. J., Elsworth, Y., Isaak, G. R., New, R., 1998, in *Structure and dynamics of the interior of the Sun and Sun-like stars: SOHO6/GONG98*, eds. S. Korzennik & A. Wilson, ESA SP-418, 6

Chaplin, W. J., Elsworth, Y., Isaak, G. R., Miller, B. A.,& New, R. 1999, MNRAS, in press

Davenport, W.B., Jr & Root, W.L., 1958, in *An introduction to the theory of random signals and noise*, International Student Edition, McGraw-Hill Book Company Inc., New York, USA

Gabriel, M. 1994, A&A, 287, 685

Harvey, J. W. 1988, in *Seismology of the Sun and Sun-Like Stars*, eds V.Domingo & E.Rolfe, ESA SP-286, 55

Hill, F., Stark, P.B., Stebbins, R.T. et al. , 1996, Science, 272, 1292

Jiménez, A., Hernandez, F. P., Claret, A., Pallé, P. L., Régulo, C.,& Cortés, T. R. 1994, ApJ, 435, 874

Kosovichev, A. G., Schou, J., Scherrer, P. H., Bogart, R. S., Bush, R. I., Hoeksema, J. T., Aloise, J., Bacon, L., Burnette, A., De Forest, C., Giles, P. M., Leibrand, K., Nigam, R., Rubin, M., Scott, K., Williams, S. D., Basu, S., Christensen-Dalsgaard, J., Däppen, W., Rhodes, E. J., Jr, Duvall, T. L., Jr, Howe, R., Thompson, M. J., Gough, D. O., Sekii, T., Toomre, J., Tarbell, T. D., Title, A. M., Mathur, D., Morrison, M., Saba, J. L. R., Wolfson, C. J., Zayer, I., & Milford, P. N. 1997, Sol. Phys., 170, 43

Loudagh, S., Provost, J., Berthomieu, G., Ehgamberdiev, S., Fossat, E., Gelly, B., Grec, G., Khalikov, S., Lazrek, M., Pallé, P., Régulo, C., Sanchez, L., & Schmider, F-X. 1993, A&A, 275, L25

Press, W.H., Teukolvsky, S.A., Vetterling, W.T. & Flannery, B.P., 1986, in *Numerical Recipes in Fortran 77*, 2nd edition, Cambridge University Press, Cambridge, UK

Quenouille, M.H., 1956, Biometrika, 43, 353

Sekii, T., 1997, in *Sounding Solar and Stellar Interiors*, eds. G. Berthomieu, J. Provost and F.X. Schmider (Kluwer Academic), 189

Toutain, T. & Appourchaux, T. 1994, A&A, 289, 649

Toutain, T. & Fröhlich, C. 1992, A&A, 257, 287

Toutain, T. & Kosovichev, A. G. 1994, A&A, 284, 265

Tomczyk, S., Streander, K., Card, G., Elmore, D., Hull, H. & Cacciani, A. 1995, Sol. Phys., 159, 1

Tomczyk, S., Schou, J. & Thompson, M.J., 1996, ApJ, 488, L57

Veitzer, S.A., Tomczyk, S.& Schou, J. 1993, ASP Conf. Ser. 42: GONG 1992. Seismic Investigation of the Sun and Stars, 465